Preassociated apocalmodulin mediates Ca^{2+}-dependent sensitization of activation and inactivation of TMEM16A/16B Ca^{2+}-gated Cl^- channels

Tingting Yang[a,1], Wayne A. Hendrickson[a,b,1], and Henry M. Colecraft[b,1]

Departments of [a]Biochemistry and Molecular Biophysics and [b]Physiology and Cellular Biophysics, College of Physicians and Surgeons, Columbia University, New York, NY 10032

Contributed by Wayne A. Hendrickson, November 6, 2014 (sent for review January 29, 2014)

Ca^{2+}-activated chloride currents carried via transmembrane proteins TMEM16A and TMEM16B regulate diverse processes including mucus secretion, neuronal excitability, smooth muscle contraction, olfactory signal transduction, and cell proliferation. Understanding how TMEM16A/16B are regulated by Ca^{2+} is critical for defining their (patho)/physiological roles and for rationally targeting them therapeutically. Here, using a bioengineering approach—channel inactivation induced by membrane-tethering of an associated protein (ChIMP)—we discovered that Ca^{2+}-free calmodulin (apoCaM) is preassociated with TMEM16A/16B channel complexes. The resident apoCaM mediates two distinct Ca^{2+}-dependent effects on TMEM16A, as revealed by expression of dominant-negative CaM_{1234}. These effects are Ca^{2+}-dependent sensitization of activation (CDSA) and Ca^{2+}-dependent inactivation (CDI). CDI and CDSA are independently mediated by the N and C lobes of CaM, respectively. TMEM16A alternative splicing provides a mechanism for tuning apoCaM effects. Channels lacking splice segment *b* selectively lost CDI, and segment *a* is necessary for apoCaM preassociation with TMEM16A. The results reveal multidimensional regulation of TMEM16A/16B by preassociated apoCaM and introduce ChIMP as a versatile tool to probe the macromolecular complex and function of Ca^{2+}-activated chloride channels.

calmodulin | anoctamin1 | TMEM16A | calcium-activated chloride channel

Calcium (Ca^{2+})-activated chloride (Cl^-) channels (CaCCs) broadly expressed in mammalian cells regulate diverse physiological functions including: epithelial mucus secretion (1, 2), neuronal excitability (3–5), smooth muscle contraction (6), olfactory transduction (7, 8), and cell proliferation (9, 10). Drugs targeting CaCCs are being pursued as therapies for hypertension, cystic fibrosis, asthma, and cancer (1, 9, 11).

Three laboratories independently identified the transmembrane protein TMEM16A as the molecular component of a CaCC (12–14). TMEM16A belongs to a protein family with 10 members encoded by distinct genes (15–18). There is universal agreement that TMEM16A, and the closely related TMEM16B, are bona fide CaCCs (2, 12–14, 19). Consistent with this, *TMEM16A* knockout mice displayed defective CaCC activity in a variety of epithelia (20–22), and the olfactory CaCC current was completely abolished in *TMEM16B* knockout mice (23). Hydropathy analyses suggest TMEM16 proteins have a similar topology with cytosolic N and C termini and eight predicted transmembrane helices (2, 19). Human TMEM16A has four alternatively spliced segments (*a–d*), differential inclusion of which modify voltage and Ca^{2+} sensitivity of resultant channel splice variants (24).

CaCCs are highly sensitive to intracellular [Ca^{2+}], displaying graded increases in Cl^- current (I_{Cl}) amplitude as $[Ca^{2+}]_i$ is raised from resting levels (~100 nM) to the 1- to 2-μM range. In some cases, high $[Ca^{2+}]_i$ (>10 μM) leads to decreased I_{Cl} amplitude (inactivation) (25–27). The Ca^{2+} sensor(s) for Ca^{2+}-dependent activation and inactivation (CDA and CDI) of TMEM16A/16B is unknown. There are two possible nonexclusive mechanisms: (*i*) direct Ca^{2+} binding to the channel or (*ii*) Ca^{2+} binding through a separate Ca^{2+}-sensing protein. The TMEM16A sequence does not reveal any canonical Ca^{2+}-binding EF hand motifs (14, 16, 17). A sequence in the first intracellular loop of TMEM16A resembling the "Ca^{2+} bowl" in large conductance Ca^{2+}-activated K^+ (BK) channels was disqualified by mutagenesis as the Ca^{2+} sensor responsible for CDA of TMEM16A (28). A revised TMEM16A topological model suggests the originally predicted extracellular loop 4 is located intracellularly (29), and mutating E702 and E705 within this loop markedly alter Ca^{2+} sensitivity of TMEM16A (29, 30).

Some reports have suggested involvement of calmodulin (CaM) in distinct aspects of Ca^{2+}-dependent regulation of CaCCs. Tian et al. reported that inhibiting CaM with trifluoperazine or J-8 markedly suppressed CDA of TMEM16A(abc) in HEK293 cells, and mapped the CaM binding site to splice segment *b* (31). They concluded that CaM is essential for TMEM16A activation. However, this suggestion is contradicted by the robust CDA of TMEM16A(ac), a splice variant lacking the putative CaM binding site on splice segment *b* (2, 24). Recently, Ca^{2+}–CaM was found to bind TMEM16A(ac) in a Ca^{2+}-dependent manner and result in an increased permeability of the channel to HCO_3^- (32). Deleting the Ca^{2+}–CaM binding site did not affect CDA of TMEM16A(ac). Ca^{2+}–CaM regulation of TMEM16A HCO_3^- permeability conforms to a traditional signaling mode where Ca^{2+} binds to freely diffusing CaM to form a Ca^{2+}–CaM complex that then interacts with a target protein.

There are several examples of an alternative mode of CaM signaling in which Ca^{2+}-free CaM (apoCaM) is preassociated with target proteins under resting $[Ca^{2+}]_i$ conditions and acts as a

Significance

Calcium-activated chloride channels (CaCCs) encoded by transmembrane members 16A and 16B (TMEM16A/16B) are vital for physiological functions ranging from smooth muscle contraction to cell proliferation and are important therapeutic targets. Here, applying a recently developed bioengineering approach referred to as channel inactivation induced by membrane tethering of an associated protein (ChIMP), we found that the Ca^{2+}-sensing protein calmodulin (CaM) is preassociated with TMEM16A/16B channel complexes in its Ca^{2+}-free state (apoCaM). The preassociated apoCaM acts as a resident Ca^{2+} sensor that increases Ca^{2+} sensitivity of TMEM16A/16B activation at low intracellular Ca^{2+} concentrations and also mediates inactivation of TMEM16A channels at high Ca^{2+} concentrations. The results reveal a previously unidentified role for apoCaM in Ca^{2+}-dependent regulation of TMEM16A/16B channels that is likely physiologically important, and may be a promising site to target for therapy.

Author contributions: T.Y., W.A.H., and H.M.C. designed research; T.Y. performed research; T.Y. and H.M.C. analyzed data; and T.Y., W.A.H., and H.M.C. wrote the paper.

The authors declare no conflict of interest.

[1]To whom correspondence may be addressed. Email: wayne@xtl.cumc.columbia.edu, ty2190@columbia.edu, or hc2405@columbia.edu.

This article contains supporting information online at www.pnas.org/lookup/suppl/doi:10.1073/pnas.1420984111/-/DCSupplemental.

resident Ca^{2+} sensor to regulate function of the host protein in response to increased $[Ca^{2+}]_i$ (33). This mode of CaM signaling is used as the activating mechanism for small conductance K^+ channels (34) and Ca^{2+}-dependent regulation of high voltage-gated Ca^{2+} (Ca_V1 and Ca_V2) channels (35, 36). A distinguishing feature of this mode of CaM signaling is that it is impervious to pharmacological inhibitors of Ca^{2+}–CaM, but can be eliminated in dominant negative fashion by a CaM mutant, CaM_{1234}, in which all four EF hands have been mutated so they no longer bind Ca^{2+} (34, 36). Whether apocalmodulin preassociates with TMEM16A/TMEM16B channel complexes and participates in Ca^{2+}-dependent regulation of these channels is controversial (30, 37, 38).

Using a recently developed bioengineering approach—channel inactivation induced by membrane-tethering of an associated protein (ChIMP) (39)—we discovered that apoCaM is functionally preassociated with TMEM16A/16B channel complexes. Whereas the resident apoCaM is not necessary for CDA, it does mediate two distinct Ca^{2+}-dependent processes in TMEM16A. First, it causes a leftward shift in the Ca^{2+}-dependent activation curve at $[Ca^{2+}]_i \leq 1$ μM, an effect we term Ca^{2+}-dependent "sensitization" of activation (CDSA). Second, it is the Ca^{2+} sensor for CDI observed at $[Ca^{2+}]_i > 10$ μM. The two opposite effects are independently mediated by the two lobes of preassociated apoCaM— Ca^{2+} occupancy of the N lobe leads to CDI, whereas the C lobe mediates CDSA. Alternative splicing of TMEM16A provides a mechanism for regulating apoCaM binding and signaling. TMEM16A splice variants lacking segment *a* lost apoCaM binding altogether, eliminating both CDSA and CDI, whereas variants specifically lacking segment *b* were selectively deficient in CDI. Finally, TMEM16A variants defective in apoCaM binding displayed dramatically decreased trafficking to the cell surface.

Results

Bioengineering Approach Reveals TMEM16A/apoCaM Preassociation. Previous biochemical pull-down studies suggest that TMEM16A does not bind apoCaM (32, 40). Additionally, whether TMEM16A binds Ca^{2+}–CaM is controversial— some biochemical pull-down studies support an interaction (31, 32), whereas others do not (40). Notably, pull-down methods can be notoriously inconsistent with regards to confirming apoCaM/Ca^{2+}–CaM association with ion channels even when these are functionally known to occur (35, 41). Purified TMEM16A(abc) was demonstrated to not bind Ca^{2+}–CaM in vitro (30). However, this result does not preclude the possibility of CaM interacting with TMEM16A channel complexes in vivo, in a manner that is functionally important. We sought to use an assay that could potentially test for association of apoCaM/Ca^{2+}–CaM with functioning TMEM16A in living cells. We recently discovered that voltage-dependent Ca^{2+} (Ca_V) channels can be inducibly inactivated by membrane tethering cytoplasmic proteins that associate either directly or indirectly with intracellular domains of the channel (39, 42). Again, we have termed this process "channel inactivation induced by membrane-tethering of an associated protein" (ChIMP). We wondered whether ChIMP would similarly work in the unrelated TMEM16A, and thus provide a new functional method for probing the macromolecular complex of this channel. To test this notion, we fused the C1 domain of protein kinase Cγ to the C terminus of CaM and coexpressed the resulting construct, $CaM–C1_{PKC}$, with TMEM16A(abc) in HEK293 cells. The hypothesis was that $CaM–C1_{PKC\gamma}$ would be induced to associate with the membrane with phorbol ester (phorbol-12,13-dibutyrate, PdBu), and if the modified CaM was bound intracellularly to TMEM16A (abc), either directly or through an intermediary, its induced membrane targeting might produce a conformational change that altered current amplitude, possibly due to an allosteric regulation of the channel pore (Fig. 1*A*). We first performed a series of control experiments. HEK293 cells transiently transfected with TMEM16A (abc) alone displayed robust outward currents in response to +100-mV step depolarizations with 1.2 μM intracellular free Ca^{2+} (Fig. 1*B*). Untransfected HEK293 cells yielded no currents, and the recorded TMEM16A(abc) currents were markedly inhibited by 100 μM niflumic acid, a nonselective CaCC blocker (13, 14) (Fig. S1*A*). Exposure to 1 μM PdBu had no impact on I_{Cl} in cells expressing TMEM16A(abc) alone (Fig. 1*B*). This result indicates that PdBu itself does not affect TMEM16A(abc) either directly or via activation of a second messenger pathway, clearing the way for using this phorbol ester in the ChIMP assay.

Cells coexpressing TMEM16A(abc) and $mCherry–CaM–C1_{PKC}$ displayed basal outward Cl^- currents with waveforms similar to those observed with TMEM16A(abc) alone (Fig. 1*C*). Remarkably, exposure to 1 μM PdBu decreased I_{Cl} amplitude concomitantly with $mCherry–CaM–C1_{PKC}$ targeting to the plasma membrane (Fig. 1*C*). We believe that the PdBu-induced decrease in I_{Cl} effect is due to direct anchoring of Ca^{2+}–CaM to the cell membrane, which induces a conformational change in the associated channel to inhibit current, as illustrated by the ChIMP concept (Fig. 1*A*). One prediction of this model is that under favorable relative expression conditions, $mCherry–CaM–C1_{PKC}$ (or mCherry–CaM) might be expected to be enriched at the plasma membrane in the

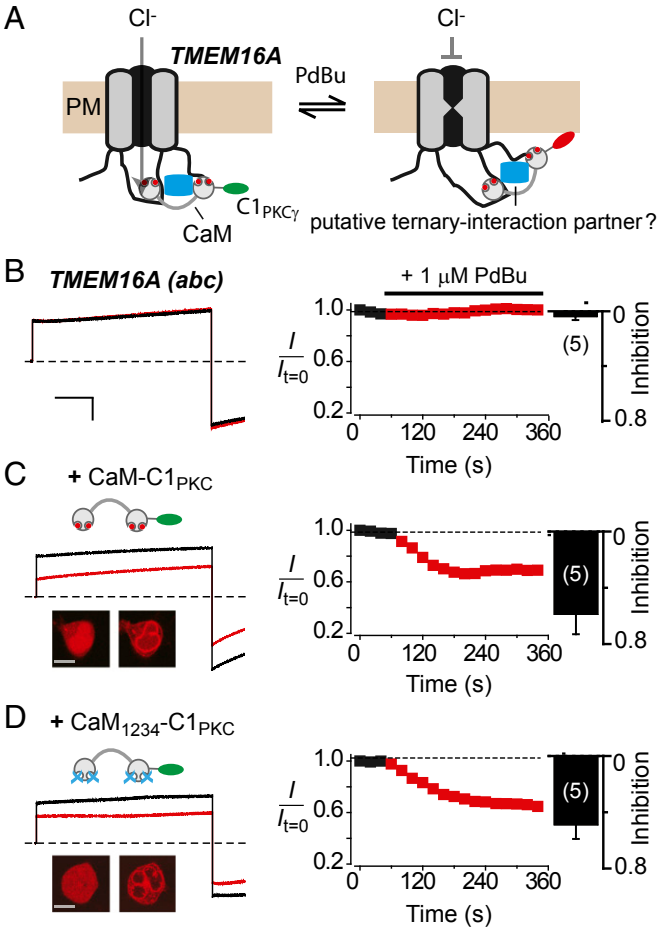

Fig. 1. A bioengineering approach reveals apoCaM preassociation with TMEM16A channel complex. (*A*) Conceptualization of the ChIMP assay. It is hypothesized that PdBu-induced membrane anchoring of $CaM–C1_{PKC\gamma}$ will regulate gating of TMEM16A if the two proteins are present in the same macromolecular complex. (*B*, *Left*) Exemplar currents elicited with 1.2 μM intracellular free Ca^{2+} before (black trace) and after (red trace) exposure to PdBu in a HEK293 cell transfected with only TMEM16A(abc). (*Right*) Diary plots and population bar chart showing PdBu does not affect TMEM16A(abc) channels. (Scale bar, 10 nA, 200 ms.) (*C*) Data for cells coexpressing TMEM16A (abc) + $CaM-C1_{PKC\gamma}$; same format as *B*. (*Inset*) Confocal image showing PdBu-induced translocation of $mCherry–CaM–C1_{PKC}$ from cytosol to the plasma membrane in a transfected HEK293 cell. (Scale bar, 5 μm.) (*D*) Data for cells coexpressing TMEM16A(abc) + $mCherry–CaM_{1234}–C1_{PKC}$; same format as *C*.

absence of PdBu due to its putative association with membrane-bound TMEM16A(abc) channel complex. Indeed, we observed evidence of such membrane enrichment of mCherry–CaM with TMEM16A–GFP (Fig. S1*B*). To test for a possible preassociation of apoCaM, we used a Ca^{2+}-insensitive CaM mutant, CaM_{1234}, in the ChIMP assay. Cells coexpressing TMEM16A (abc) and mCherry–CaM_{1234}–$C1_{PKC}$ expressed large currents that were also sharply inhibited by 1 μM PdBu (Fig. 1*D*), providing to our knowledge the first evidence of putative apoCaM preassociation with functioning TMEM16A(abc) channel complexes in live cells. As a negative control, cells expressing TMEM16A(abc) and $C1_{PKC}$-fused Ca_V channel auxiliary β_3 subunit (β_3–$C1_{PKC}$, a protein that does not bind TMEM16A) displayed currents that were unaffected by PdBu (Fig. S1*C*).

Because TMEM16A(abc) coexpressed with mCherry–CaM_{1234}–$C1_{PKC}$ still produced large I_{Cl} (Fig. 1*D*), we could formally rule out the idea that the preassociated apoCaM is the Ca^{2+} sensor for CDA of TMEM16A. This is in full agreement with recent data indicating that CaM is not the Ca^{2+} sensor for CDA of TMEM16A (30, 32, 37). Nevertheless, we were motivated by the ChIMP results to probe whether apoCaM preassociated with the TMEM16A(abc) channel complex plays any role in Ca^{2+}-dependent regulation of these channels.

Preassociated apoCaM Mediates Two Distinct Processes in TMEM16A. To test for other possible functions of preassociated apoCaM in regulation of TMEM16A, we compared the impact of wild-type (WT) CaM and CaM_{1234} on CDA and CDI of TMEM16A(abc) across a range of free $[Ca^{2+}]_i$. As baseline, HEK293 cells transfected with TMEM16A(abc) alone displayed Ca^{2+}- and voltage-dependent Cl^- currents that increased in amplitude as $[Ca^{2+}]_i$ was raised from 93 nM to 1.2 μM (Fig. 2 *A* and *B*), in agreement with previous reports (12–14). When $[Ca^{2+}]_i$ was raised to 17 μM, I_{Cl} amplitude was lower than that obtained with 1.2 μM Ca^{2+} (Fig. 2 *A* and *B*). A plot of peak current (evoked with a 100-mV step pulse) as a function of $[Ca^{2+}]_i$ displayed a biphasic profile consistent with two distinct Ca^{2+}-dependent processes—CDA occurs between 93 nM and 1.2 μM $[Ca^{2+}]_i$, whereas CDI is seen with $[Ca^{2+}]_i$ at 17 μM (Fig. 2*D*, open triangle). Coexpressing WT CaM with TMEM16A(abc) produced a virtually identical profile of CDA and CDI as observed with TMEM16A(abc) alone (Fig. 2 *C* and *D*, filled square). In contrast, we observed two clear-cut effects of CaM_{1234} on Ca^{2+}-dependent regulation of TMEM16A (abc) (Fig. 2*C*, red square). First, there was a rightward shift in Ca^{2+} dependence of activation at $[Ca^{2+}]_i \leq 1.2$ μM for TMEM16A(abc) coexpressed with CaM_{1234}, compared with those expressed either alone or with WT CaM (Fig. 2 *C* and *D*). Second, with CaM_{1234}, CDI was eliminated (Fig. 2*D*, red square). Assuming that CaM_{1234} exerts dominant negative effects by displacing endogenous apoCaM from their binding sites, these results suggest that preassociated apoCaM is the Ca^{2+} sensor for CDSA and CDI of TMEM16A(abc).

ApoCaM N and C Lobes Independently Mediate TMEM16A CDI and CDSA. The Ca^{2+} dependence of TMEM16A(abc) CDSA and CDI span approximately two orders of magnitude, raising the question of how preassociated apoCaM is able to act as the Ca^{2+} sensor for two divergent functional responses across this wide range of $[Ca^{2+}]_i$. This situation has parallels with CaM regulation of $Ca_V2.1$ channels, where preassociated CaM similarly decodes Ca^{2+} signals to produce two functionally opposite effects on the channel—Ca^{2+}-dependent facilitation (CDF) and CDI (43). Strikingly, $Ca_V2.1$ channel CDI and CDF were found to be mediated independently by the N and C lobes of CaM, respectively (43). We wondered whether a similar CaM lobe-specific bifurcation of Ca^{2+} signals was at play in mediating TMEM16A(abc) CDSA and CDI. To test this idea, we coexpressed TMEM16A(abc) with mutant CaMs in which Ca^{2+} sensitivity of either the N lobe (CaM_{12}) or C lobe (CaM_{34}) was eliminated (34, 43).

TMEM16A(abc) coexpressed with CaM_{12} displayed I_{Cl} with a $[Ca^{2+}]_i$-dependent activation profile that indicated the preservation of CDSA, but a complete loss of CDI (Fig. 3*A*, blue square). Conversely, TMEM16A(abc) coexpressed with CaM_{34} selectively lost CDSA while leaving CDI intact (Fig. 3*B*, green square). These results demonstrate that the N lobe of CaM selectively mediates TMEM16A(abc) CDI, whereas the C lobe transduces CDSA.

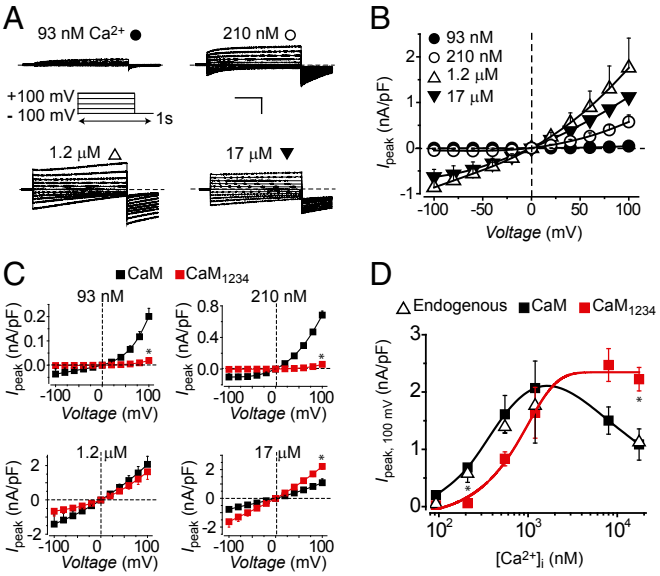

Fig. 2. Preassociated apoCaM mediates two distinct Ca^{2+}-dependent processes in TMEM16A(abc). (*A*) Representative I_{Cl} traces recorded from HEK293 cells transfected with TMEM16A(abc) at various free intracellular Ca^{2+} concentrations. Voltage protocol used to elicit currents is shown in *Inset*. (Scale bar, 10 nA, 200 ms.) (*B*) Population steady-state current–voltage (I_{peak}–*V*) relationships at different free $[Ca^{2+}]_i$; n = 5–9 for each point. (*C*) Population I_{peak}–*V* relationships for TMEM16A(abc) coexpressed with either WT CaM (■) or CaM_{1234} (red square); n = 5 for each point. *$P < 0.05$ compared with TMEM16A(abc) + CaM using two-tailed unpaired Student *t* test. (*D*) $[Ca^{2+}]_i$ dependence of TMEM16A(abc) activation. Steady-state current density recorded at +100 mV plotted vs. free $[Ca^{2+}]_i$ for TMEM16A(abc) expressed alone (open triangle) or with either WT CaM (■) or CaM_{1234} (red square); n = 5–9 for each point.

Role of TMEM16A Splice Segments in apoCaM Regulation. The *TMEM16A* gene has four alternatively spliced segments designated *a*–*d*, which are predicted to be intracellular and confer distinctive biophysical properties to TMEM16A splice variants (Fig. 4*A*) (12, 24). Because distinct TMEM16A splice variants are expressed in different tissues (24), dissecting their functional properties is crucial for understanding tissue-specific modulation of CaCCs. We determined whether and how the individual segments *a*, *b*, and *c* impact apoCaM binding and regulation of TMEM16A.

First, we examined functional properties of TMEM16A(ac), which specifically lacks segment *b*. When coexpressed with WT CaM, CDA of TMEM16A(ac) closely tracked that of TMEM16A (abc) for $[Ca^{2+}]_i \leq 1.2$ μM (Fig. 4*B*, black square), although with 93 nM and 210 nM $[Ca^{2+}]_i$, TMEM16A(ac) tended to have a larger I_{Cl} amplitude compared with TMEM16A(abc) (Fig. S2), consistent with previous observations (24). Notably, with 17 μM $[Ca^{2+}]_i$, TMEM16A(ac) displayed no CDI, clearly diverging from TMEM16A(abc) under this condition (Fig. 4*B* and Fig. S2). When coexpressed with CaM_{1234}, TMEM16A(ac) currents elicited at 93 nM and 210 nM displayed a significantly lower amplitude compared with WT CaM (Fig. 4*B* and Fig. S3) and showed a CDA profile that overlaid that of TMEM16A(abc) + CaM_{1234} (Fig. 4*B*, red square). These results indicate that CDSA is preserved in TMEM16A(ac), whereas CDI is selectively lost. Hence, segment *b* is necessary for preassociated apoCaM-mediated CDI of TMEM16A.

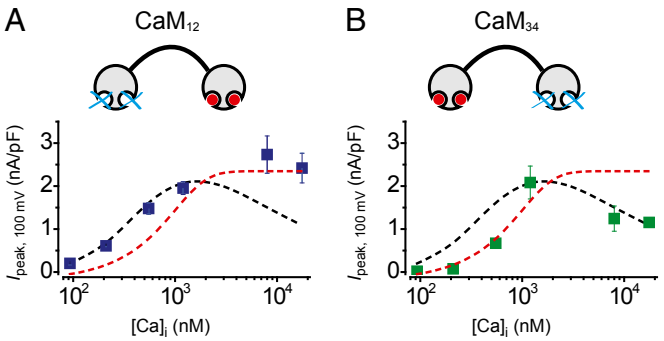

Fig. 3. The N and C lobes of preassociated apoCaM independently mediate CDI and CDSA of TMEM16A(abc). (*A*, *Top*) Schematic of CaM_{12}. (*Bottom*) Steady-state current density recorded at +100 mV plotted vs. free $[Ca^{2+}]_i$ for TMEM16A(abc) coexpressed with CaM_{12} (blue square). Curves for TMEM16A (abc) + WT CaM (dotted black line) and TMEM16A (abc) + CaM_{1234} (dotted red line) are reproduced from Fig. 2*D* to facilitate visual comparison; $n = 5$ for each point. (*B*) Data for TMEM16A(abc) + CaM_{34} (green square), same format as *A*; $n = 5$ for each point.

Next, we investigated the properties of TMEM16A(0), which lacks all of the alternatively spliced segments. As previously reported (25), this minimal TMEM16A isoform supported Ca^{2+}-activated chloride currents (Fig. S2). However, even when coexpressed with WT CaM, the activation profile of TMEM16A(0) tracked that of TMEM16A(abc) + CaM_{1234} (Fig. 4*C*, black square). Therefore, TMEM16A(0) lacks both CDSA and CDI, the two functional signatures of preassociated apoCaM.

The simplest interpretation of the data with the two TMEM16A variants is that apoCaM preassociates with TMEM16A(ac) but not TMEM16A(0) channel complexes. To test this idea, we used ChIMP to gain further insights into which TMEM16A splice variants associate with apoCaM. TMEM16A(ac) coexpressed with CaM–$C1_{PKC}$ or CaM_{1234}–$C1_{PKC}$ gave rise to Ca^{2+}-activated I_{Cl} that were rapidly inhibited by PdBu (Fig. 4*D* and Fig. S4). By contrast, I_{Cl} from TMEM16A(0) coexpressed with CaM–$C1_{PKC}$ was insensitive to PdBu (Fig. 4*E*). The effectiveness of ChIMP for TMEM16A(ac) but not TMEM16A(0) suggested that segments *a* and/or *c* are important for apoCaM binding to TMEM16A. To further dissect whether one or both of these segments is essential for apoCaM binding, we used ChIMP to probe TMEM16A(a) and TMEM16A(c), respectively. When coexpressed with CaM–$C1_{PKC}$ or CaM_{1234}–$C1_{PKC}$, currents through TMEM16A(a) were blocked by Pdbu (Fig. 4*F* and Fig. S4), whereas TMEM16A(c) currents were insensitive to PdBu (Fig. 4*G*). In control experiments, neither TMEM16A(ac) nor TMEM16A(a) expressed alone was responsive to PdBu (Fig. S4).

A large fraction (~70%) of cells transfected with either GFP-tagged TMEM16A(0) or TMEM16A(c) yielded no currents, whereas the remaining 30% displayed Ca^{2+}-activated I_{Cl} that lack CDSA. By contrast, cells expressing GFP-tagged TMEM16A (abc), TMEM16A(ac), or TMEM16A(a) always displayed robust Ca^{2+}-activated I_{Cl}. This variance may be explained by differences in channel trafficking to the cell surface, as we found that channels lacking segment *a* were poorly targeted to the plasma membrane (Fig. S5).

Biochemical Detection of apoCaM Binding to TMEM16A Variants. We used coimmunoprecipitation assays to directly confirm that apoCaM physically binds TMEM16A channel complex, and that segment *a* is necessary for this interaction. Different GFP-tagged TMEM16A splice variants were coexpressed with Xpress-tagged YFP–CaM in HEK293 cells. In agreement with the ChIMP data, we found that TMEM16A(abc), TMEM16A(ac), and TMEM16A (a) coimmunoprecipitated with CaM, whereas TMEM16A(c) and TMEM16A(0) did not, in the absence or presence of Ca^{2+} (Fig. 5 *A* and *B*). We further found that Xpress–YFP–CaM_{1234} coimmunoprecipitated with TMEM16A(abc), TMEM16A(ac), and TMEM16A(a), directly confirming apoCaM preassociation with these channels (Fig. 5*C*). As a negative control, GFP did not coimmunoprecipitate with Xpress–YFP–CaM_{1234}. Taken together, the results indicate that segment *a* is necessary for apoCaM binding to TMEM16A channel complex. We were unable to pull down the isolated TMEM16A intracellular N terminus (which contains segment *a*) with CaM (Fig. S6), suggesting segment *a* is necessary but not sufficient for apoCaM binding to the channel complex.

Discussion

The previously unknown results provided in this work are: (*i*) apoCaM is preassociated with TMEM16A/16B channel complexes (Fig. S7) at resting $[Ca^{2+}]_i$; (*ii*) the preassociated apoCaM mediates CDSA and CDI of TMEM16A(abc); (*iii*) CaM N and C lobes independently mediate CDI and CDSA, respectively; (*iv*) TMEM16A alternatively spliced segments *a* and *b* are necessary for apoCaM binding and CDI, respectively; and (*v*) the ChIMP

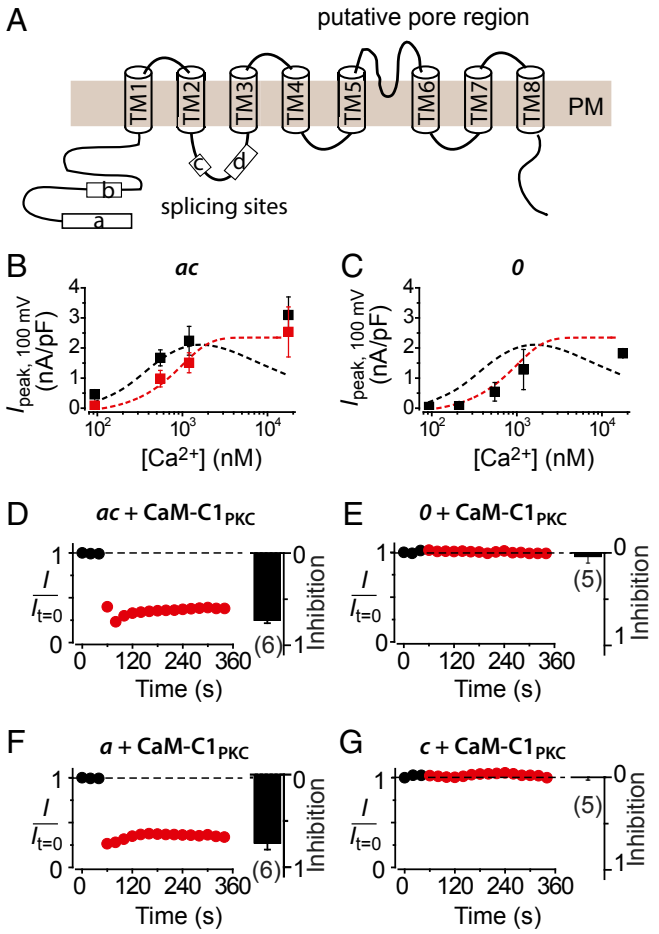

Fig. 4. Dissecting the role of TMEM16A alternatively spliced segments in apoCaM-dependent modulation. (*A*) Predicted topology of TMEM16A and location of alternatively spliced segments *a*–*d*. (*B*) Steady-state current density recorded at +100 mV plotted vs. free $[Ca^{2+}]_i$ for TMEM16A(ac) coexpressed with either WT CaM (■) or CaM_{1234} (red square). Curves for TMEM16A(abc) + CaM (dotted black line) and TMEM16A (abc) + CaM_{1234} (dotted red line) are reproduced from Fig. 2*D* to facilitate visual comparison; $n = 5$–6 for each point. (*C*) Data for cells TMEM16A(0) + WT CaM (■), same format as *B*; $n = 5$–9 for each point. (*D*) ChIMP assay. Diary plots and population bar chart showing effect of 1 μM PdBu on TMEM16A(ac) coexpressed with mCherry–CaM–$C1_{PKC}$. (*E*–*G*) Data for TMEM16A(0), TMEM16A(a), and TMEM16A(c); same format as *D*.

assay is an effective tool to probe and manipulate TMEM16A/16B. We discuss these aspects of our results in relation to previous work with emphasis on structure–function mechanisms, physiological implications, and potential pharmacological applications.

In agreement with previous results, our data show that preassociated apoCaM is not the Ca^{2+}-sensor responsible for CDA of TMEM16A/16B. Beyond CDA, however, TMEM16A/16B display other Ca^{2+}-regulated gating and permeation processes through a direct interaction with Ca^{2+}–CaM as shown by this and other studies. In particular, the CDI phenomenon has previously been observed (25, 26), although the Ca^{2+} sensor for this process was unknown. Interestingly, reconstituted purified TMEM16A (abc) lacks CDI, suggesting the sensor for this phenomenon is not encoded within the channel's primary sequence (30). Recent studies indicate that Ca^{2+}–CaM regulates the HCO_3^- permeability (32) and run-up/run-down of TMEM16A (40). These modes of CaM signaling are different from what we report here, which features apoCaM preassociated to TMEM16A/16B channel complexes as a resident Ca^{2+} sensor. The functional effects of overexpressing CaM_{1234} reveal that preassociated apoCaM is the Ca^{2+} sensor for CDI in TMEM16A(abc). Our results also revealed a previously unidentified form of Ca^{2+}-dependent regulation of TMEM16A, CDSA, which is also mediated by the preassociated apoCaM. Interestingly, CDI and CDSA were independently mediated through Ca^{2+}-binding to the N and C lobes, respectively, of the resident apoCaM. This profile fits nicely with the known differential affinity of the two lobes of CaM for Ca^{2+} (N lobe, K_d ~12 μM; C lobe, K_d ~1 μM) (33, 44). The lobe specificity is reminiscent of CaM regulation of $Ca_V2.1$ channels, where preassociated apoCaM uses N and C lobes to bifurcate Ca^{2+} signals to produce CDI and CDF, respectively (43). To our knowledge, this work provides only the second example of a resident apoCaM splitting the Ca^{2+} signal to produce opposite functional readouts on a host channel.

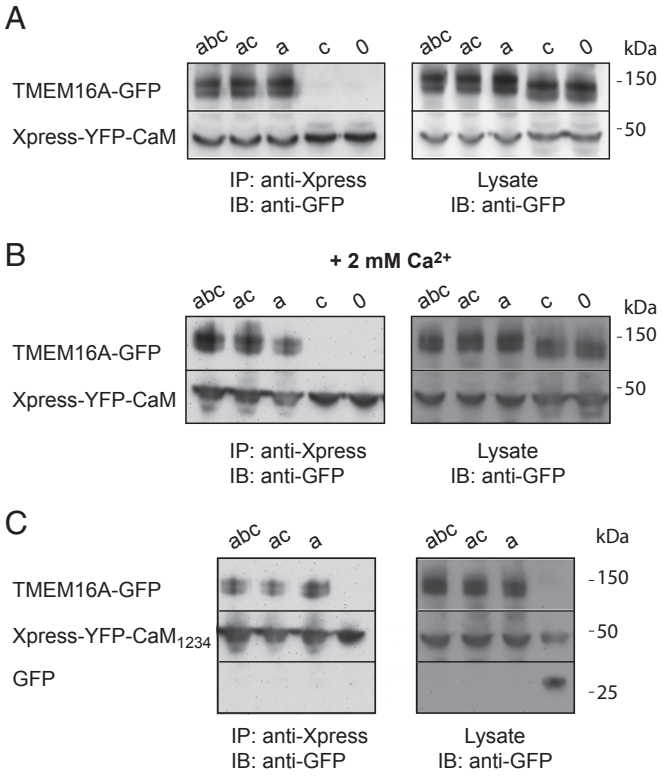

Fig. 5. Coimmunoprecipitation of CaM with TMEM16A variants. (*A*) Coimmunoprecipitation of distinct GFP-tagged TMEM16A splice variants with Xpress–YFP–CaM at basal Ca^{2+}. (*B*) Coimmunoprecipitation of distinct GFP-tagged TMEM16A splice variants with Xpress–YFP–CaM at 2 mM Ca^{2+}. (*C*) Coimmunoprecipitation of distinct GFP-tagged TMEM16A splice variants with Xpress–YFP–CaM_{1234}.

We initially inferred a TMEM16A–apoCaM interaction based on successful functional outcomes of the ChIMP assay with CaM_{1234}–$C1_{PKC}$ for TMEM16A splice variants. This intuition was explicitly confirmed by coimmunoprecipitation assays in which all TMEM16A splice variants containing segment *a* were successfully pulled down with apoCaM. Tian et al. also demonstrated that CaM and TMEM16A(abc) coimmunoprecipitated together when coexpressed in HEK293 cells (31). They inferred that splice segment *b* was important for the TMEM16A–CaM interaction by showing that TMEM16A(ac) can no longer be pulled down with CaM. By contrast, we found that segment *a* rather than segment *b* is essential for apoCaM binding to TMEM16A. The reason for the discrepant results is unclear. Surprisingly, we were unable to coimmunoprecipitate the entire intracellular TMEM16A N terminus with CaM. This may indicate that CaM binds stably to the holo channel using multiple weak binding sites including at least one located in segment *a*. Alternatively, segment *a* could be necessary by promoting a conformation of TMEM16A that exposes the apoCaM binding site elsewhere on the channel. It is also possible that apoCaM does not bind directly to TMEM16A, but associates with the channel complex through an intermediary protein. This scenario would be consistent with the observation that purified TMEM16A does not associate with CaM (30). Notably, Jung et al. identified Ca^{2+}-dependent CaM binding to TMEM16A using pull-down assays (32). In contrast to our results, they did not observe CaM binding to TMEM16A under Ca^{2+}-free conditions. This fundamental difference in observations is most likely explained by variation in experimental methods. Jung et al. used purified GST–CaM to pull-down TMEM16A from HEK293 cell lysates. Our results indicate that under these conditions, TMEM16A channel complex is already preassociated with endogenous apoCaM, thus possibly preventing GST–CaM access to the binding site. Taken together with previous results (32), we speculate that at least two independent CaM binding sites exist in the TMEM16A channel complex—a site for apoCaM that mediates CDSA and CDI and a separate site for Ca^{2+}–CaM that regulates channel permeability to HCO_3^-. In contrast to our results, Yu et al. were unable to coimmunoprecipitate TMEM16A with epitope-tagged CaM expressed in HEK293 cells (37). The reasons for the discrepant results are not obvious. Clearly, further work is needed to nail down the precise nature of the apoCaM binding site within the TMEM16A channel complex. Our results provide a clear functional signature of this preassociated apoCaM, which in turn provide the impetus for such future studies.

We propose that TMEM16A and TMEM16B channels in native cells have a preassociated apoCaM as part of the channel complex under resting $[Ca^{2+}]_i$. Our results suggest that without the preassociated apoCaM, the Ca^{2+} sensitivity of TMEM16A/16B activation at low to moderate $[Ca^{2+}]_i$ would be significantly lower, and thereby impact the many biological functions that depend on channel opening. Further experiments in native systems are needed to define the broad physiological implications of our findings. One previous study examined the impact of various CaM EF hand mutants on the activation of CaCCs recorded from the *Odora* cell line, which are derived from olfactory sensory neuron (OSN) precursor cells in the rat olfactory epithelium (38). They found that several CaM mutants (CaM_1, CaM_2, and CaM_{12}) shifted the Ca^{2+}-dependent activation curve of the endogenous CaCC to the right, consistent with our idea that a preassociated apoCaM mediates CDSA. Surprisingly, they observed no impact of CaM_{1234} on the Ca^{2+}-dependent activation curve of the endogenous CaCC, in contrast to our results in HEK293 cells (Fig. S7).

This study demonstrates the utility of ChIMP to probe structure–function mechanisms and regulation of TMEM16A/16B. That the ChIMP method, which was previously developed in Ca_V channels (39), is similarly effective in the unrelated TMEM16A/

BIOCHEMISTRY

16B suggests that it may be generally applicable to the study and modulation of many different ion channel families. A recent quantitative proteomic approach revealed that TMEM16A is associated with a large network of intracellular proteins, many of which could be important for channel regulation (45). The ChIMP assay could be an invaluable tool for dissecting the functional relevance of other cytosolic proteins that putatively interact with TMEM16A intracellular domains. Finally, the approach also has promise for developing novel genetically encoded inhibitors for TMEM16A and TMEM16B channels.

Materials and Methods

Detailed methods are provided in *SI Materials and Methods*.

cDNA Cloning. Mouse TMEM16A(abc), TMEM16A(ac), and TMEM16B–GFP were generous gifts from Criss Hartzell (Emory University, Atlanta). Expression plasmids were generated using PCR and standard restriction enzyme ligation and cloning strategies.

Cell Culture and Transfection. HEK293 cells maintained in DMEM supplemented with 10% (vol/vol) FBS and 100 $\mu g \cdot ml^{-1}$ penicillin–streptomycin were transfected using the calcium phosphate precipitation method.

Electrophysiology. Whole-cell recordings of HEK cells were conducted 48–72 h after transfection using an EPC8 or EPC10 patch clamp amplifier (HEKA Electronics) controlled by PULSE software (HEKA).

Confocal Microscopy. Confocal imges were acquired using a Leica TCS SPL AOBS MP confocal microscope system and a 40× oil objective (HCX PL APO 1.25–0.75 NA). HEK293 cells expressing GFP and mCherry fusion proteins were excited using the 488- and 543-nm argon laser lines, respectively.

Immunoprecipitation and Immunoblotting. For high-calcium experiments, transfected cells were preincubated for 30 min with A23187 (5 μM) in the presence of 2 mM external $CaCl_2$ before solubilization in lysis buffer (50 mmol/L Tris·HCl, 150 mmol/L NaCl, 1% IGEPAL CA-630, 2 mM $CaCl_2$). For immunoblots, primary antibodies (anti-GFP; Invitrogen) were detected by horseradish peroxidase-conjugated secondary antibodies (goat anti-rabbit; Thermo Scientific) and enhanced chemiluminescence.

Data and Statistical Analyses. Data were analyzed off-line using PulseFit (HEKA), Microsoft Excel, and Origin software. Statistical analyses were performed in Origin using built-in functions. Statistically significant differences between means ($P < 0.05$) were determined using Student t test for comparisons between two groups, or one-way ANOVA followed by pairwise means comparisons using Bonferroni test for multiple groups. Data are presented as means ± SEM.

ACKNOWLEDGMENTS. We thank Dr. H. Criss Hartzell (Emory University) for the generous gift of TMEM16A and TMEM16B plasmids; Dr. David T. Yue (Johns Hopkins University) for CaM_{1234}, CaM_{12}, and CaM_{34} cDNA; and Ming Chen for excellent technical support. This work was supported by Grant RO1 HL069911 from the National Institutes of Health (to H.M.C.). H.M.C. is an Established Investigator of the American Heart Association.

1. Huang F, et al. (2012) Calcium-activated chloride channel TMEM16A modulates mucin secretion and airway smooth muscle contraction. *Proc Natl Acad Sci USA* 109(40): 16354–16359.
2. Ferrera L, Caputo A, Galietta LJ (2010) TMEM16A protein: A new identity for Ca(2+)-dependent Cl^- channels. *Physiology (Bethesda)* 25(6):357–363.
3. Duan D (2009) Phenomics of cardiac chloride channels: The systematic study of chloride channel function in the heart. *J Physiol* 587(Pt 10):2163–2177.
4. Liu B, et al. (2010) The acute nociceptive signals induced by bradykinin in rat sensory neurons are mediated by inhibition of M-type K+ channels and activation of Ca2+-activated Cl^- channels. *J Clin Invest* 120(4):1240–1252.
5. Huang WC, et al. (2012) Calcium-activated chloride channels (CaCCs) regulate action potential and synaptic response in hippocampal neurons. *Neuron* 74(1):179–192.
6. Large WA, Wang Q (1996) Characteristics and physiological role of the Ca(2+)-activated Cl^- conductance in smooth muscle. *Am J Physiol* 271(2 Pt 1):C435–C454.
7. Reisert J, Lai J, Yau KW, Bradley J (2005) Mechanism of the excitatory Cl^- response in mouse olfactory receptor neurons. *Neuron* 45(4):553–561.
8. Hengl T, et al. (2010) Molecular components of signal amplification in olfactory sensory cilia. *Proc Natl Acad Sci USA* 107(13):6052–6057.
9. Duvvuri U, et al. (2012) TMEM16A induces MAPK and contributes directly to tumorigenesis and cancer progression. *Cancer Res* 72(13):3270–3281.
10. Stanich JE, et al. (2011) Ano1 as a regulator of proliferation. *Am J Physiol Gastrointest Liver Physiol* 301(6):G1044–G1051.
11. Verkman AS, Galietta LJ (2009) Chloride channels as drug targets. *Nat Rev Drug Discov* 8(2):153–171.
12. Caputo A, et al. (2008) TMEM16A, a membrane protein associated with calcium-dependent chloride channel activity. *Science* 322(5901):590–594.
13. Schroeder BC, Cheng T, Jan YN, Jan LY (2008) Expression cloning of TMEM16A as a calcium-activated chloride channel subunit. *Cell* 134(6):1019–1029.
14. Yang YD, et al. (2008) TMEM16A confers receptor-activated calcium-dependent chloride conductance. *Nature* 455(7217):1210–1215.
15. Flores CA, Cid LP, Sepúlveda FV, Niemeyer MI (2009) TMEM16 proteins: The long awaited calcium-activated chloride channels? *Braz J Med Biol Res* 42(11):993–1001.
16. Duran C, Thompson CH, Xiao Q, Hartzell HC (2010) Chloride channels: Often enigmatic, rarely predictable. *Annu Rev Physiol* 72:95–121.
17. Berg J, Yang H, Jan LY (2012) Ca2+-activated Cl^- channels at a glance. *J Cell Sci* 125(Pt 6):1367–1371.
18. Huang F, Wong X, Jan LY (2012) International Union of Basic and Clinical Pharmacology. LXXXV: Calcium-activated chloride channels. *Pharmacol Rev* 64(1):1–15.
19. Duran C, Hartzell HC (2011) Physiological roles and diseases of Tmem16/Anoctamin proteins: Are they all chloride channels? *Acta Pharmacol Sin* 32(6):685–692.
20. Ousingsawat J, et al. (2009) Loss of TMEM16A causes a defect in epithelial Ca2+-dependent chloride transport. *J Biol Chem* 284(42):28698–28703.
21. Rock JR, et al. (2009) Transmembrane protein 16A (TMEM16A) is a Ca2+-regulated Cl^- secretory channel in mouse airways. *J Biol Chem* 284(22):14875–14880.
22. Romanenko VG, et al. (2010) Tmem16A encodes the Ca2+-activated Cl^- channel in mouse submandibular salivary gland acinar cells. *J Biol Chem* 285(17):12990–13001.
23. Billig GM, Pál B, Fidzinski P, Jentsch TJ (2011) Ca2+-activated Cl^- currents are dispensable for olfaction. *Nat Neurosci* 14(6):763–769.
24. Ferrera L, et al. (2009) Regulation of TMEM16A chloride channel properties by alternative splicing. *J Biol Chem* 284(48):33360–33368.
25. Ferrera L, et al. (2011) A minimal isoform of the TMEM16A protein associated with chloride channel activity. *Biochim Biophys Acta* 1808(9):2214–2223.
26. Schreiber R, et al. (2010) Expression and function of epithelial anoctamins. *J Biol Chem* 285(10):7838–7845.
27. Pifferi S, Dibattista M, Menini A (2009) TMEM16B induces chloride currents activated by calcium in mammalian cells. *Pflugers Arch* 458(6):1023–1038.
28. Xiao Q, et al. (2011) Voltage- and calcium-dependent gating of TMEM16A/Ano1 chloride channels are physically coupled by the first intracellular loop. *Proc Natl Acad Sci USA* 108(21):8891–8896.
29. Yu K, Duran C, Qu Z, Cui YY, Hartzell HC (2012) Explaining calcium-dependent gating of anoctamin-1 chloride channels requires a revised topology. *Circ Res* 110(7):990–999.
30. Terashima H, Picollo A, Accardi A (2013) Purified TMEM16A is sufficient to form Ca2+-activated Cl^- channels. *Proc Natl Acad Sci USA* 110(48):19354–19359.
31. Tian Y, et al. (2011) Calmodulin-dependent activation of the epithelial calcium-dependent chloride channel TMEM16A. *FASEB J* 25(3):1058–1068.
32. Jung J, et al. (2013) Dynamic modulation of ANO1/TMEM16A HCO3(–) permeability by Ca2+/calmodulin. *Proc Natl Acad Sci USA* 110(1):360–365.
33. Saucerman JJ, Bers DM (2012) Calmodulin binding proteins provide domains of local Ca2+ signaling in cardiac myocytes. *J Mol Cell Cardiol* 52(2):312–316.
34. Xia XM, et al. (1998) Mechanism of calcium gating in small-conductance calcium-activated potassium channels. *Nature* 395(6701):503–507.
35. Erickson MG, Alseikhan BA, Peterson BZ, Yue DT (2001) Preassociation of calmodulin with voltage-gated Ca(2+) channels revealed by FRET in single living cells. *Neuron* 31(6):973–985.
36. Peterson BZ, DeMaria CD, Adelman JP, Yue DT (1999) Calmodulin is the Ca2+ sensor for Ca2+-dependent inactivation of L-type calcium channels. *Neuron* 22(3):549–558.
37. Yu K, Zhu J, Qu Z, Cui YY, Hartzell HC (2014) Activation of the Ano1 (TMEM16A) chloride channel by calcium is not mediated by calmodulin. *J Gen Physiol* 143(2):253–267.
38. Kaneko H, Möhrlen F, Frings S (2006) Calmodulin contributes to gating control in olfactory calcium-activated chloride channels. *J Gen Physiol* 127(6):737–748.
39. Yang T, He LL, Chen M, Fang K, Colecraft HM (2013) Bio-inspired voltage-dependent calcium channel blockers. *Nat Commun* 4:2540.
40. Vocke K, et al. (2013) Calmodulin-dependent activation and inactivation of anoctamin calcium-gated chloride channels. *J Gen Physiol* 142(4):381–404.
41. Müller CS, et al. (2010) Quantitative proteomics of the Cav2 channel nano-environments in the mammalian brain. *Proc Natl Acad Sci USA* 107(34):14950–14957.
42. Yang T, Suhail Y, Dalton S, Kernan T, Colecraft HM (2007) Genetically encoded molecules for inducibly inactivating CaV channels. *Nat Chem Biol* 3(12):795–804.
43. DeMaria CD, Soong TW, Alseikhan BA, Alvania RS, Yue DT (2001) Calmodulin bifurcates the local Ca2+ signal that modulates P/Q-type Ca2+ channels. *Nature* 411(6836):484–489.
44. Black DJ, Leonard J, Persechini A (2006) Biphasic Ca2+-dependent switching in a calmodulin-IQ domain complex. *Biochemistry* 45(22):6987–6995.
45. Perez-Cornejo P, et al. (2012) Anoctamin 1 (Tmem16A) Ca2+-activated chloride channel stoichiometrically interacts with an ezrin-radixin-moesin network. *Proc Natl Acad Sci USA* 109(26):10376–10381.